

Histogram of Gradient Orientations of Signal Plots applied to P300 Detection

Rodrigo Ramele^{1,*}, Ana Julia Villar¹ and Juan Miguel Santos¹

¹*Centro de Inteligencia Computacional, Computer Engineering Department, Instituto Tecnológico de Buenos Aires, Buenos Aires, Argentina*

Correspondence*:

Rodrigo Ramele, C1437FBH Lavarden 315, Ciudad Autónoma de Buenos Aires, Argentina
rramele@itba.edu.ar

2 ABSTRACT

3 Word Count: 5132

4 The analysis of Electroencephalographic (EEG) signals is of ulterior importance to aid in the
5 diagnosis of mental disease and to increase our understanding of the brain. Traditionally, clinical
6 EEG has been analyzed in terms of temporal waveforms, looking at rhythms in spontaneous
7 activity, subjectively identifying troughs and peaks in Event-Related Potentials (ERP), or by
8 studying graphoelements in pathological sleep stages. Additionally, the discipline of Brain
9 Computer Interfaces requires new methods to decode patterns from non-invasive EEG signals.
10 This field is developing alternative communication pathways to transmit volitional information
11 from the Central Nervous System. The technology could potentially enhance the quality of life
12 of patients affected by neurodegenerative disorders and other mental illness. This work mimics
13 what electroencephalographers have been doing clinically, visually inspecting and categorizing
14 phenomena within the EEG by the extraction of features from images of signal plots. These
15 features are constructed based on the calculation of histograms of oriented gradients from pixels
16 around the signal plot. It aims to provide a new objective framework to analyze, characterize and
17 classify EEG signal waveforms. The feasibility of the method is outlined by detecting the P300, an
18 ERP elicited by the oddball paradigm of rare events, and implementing an offline P300-based BCI
19 Speller. The validity of the proposal is shown by offline processing a public dataset of Amyotrophic
20 Lateral Sclerosis (ALS) patients and an own dataset of healthy subjects.

21 **Keywords:** electroencephalography, histogram of gradient orientations, brain-computer interfaces, P300, SIFT, amyotrophic lateral
22 sclerosis, naive-bayes near neighbours, waveforms

1 INTRODUCTION

23 Although recent advances in neuroimaging techniques, particularly radio-nuclear and radiological
24 scanning methods (Schomer and Silva, 2010), have diminished the prospects of the traditional
25 Electroencephalography (EEG), the advent and development of digitized devices has impelled for a
26 revamping of this hundred years old technology. Their versatility, ease of use, temporal resolution, ease of
27 development and production, and its proliferation as consumer devices, are pushing EEG to become the
28 de-facto non invasive portable or ambulatory method to access and harness brain information (De Vos and
29 Debener, 2014).

30 A key contribution to this expansion has been the field of Brain Computer Interfaces (BCI) (Wolpaw and
31 E., 2012) which is the pursuit of the development of a new channel of communication particularly aimed to
32 persons affected by neurodegenerative diseases.

33 One noteworthy aspect of this novel communication channel is the ability to transmit information from
34 the Central Nervous System (CNS) to a computer device and from there use that information to control a
35 wheelchair (Carlson and del R. Millan, 2013), as input to a speller application (Guger et al., 2009), in a
36 Virtual Reality environment (Lotte et al., 2013) or as aiding tool in a rehabilitation procedure (Jure et al.,
37 2016). The holy grail of BCI is to implement a new complete and alternative pathway to restore lost
38 locomotion (Wolpaw and E., 2012).

39 EEG signals are remarkably complex and have been characterized as a multichannel non-stationary
40 stochastic process. Additionally, they have high variability between different subjects and even between
41 different moments for the same subject, requiring adaptive and co-adaptive calibration and learning
42 procedures (Clerc et al., 2016). Hence, this imposes an outstanding challenge that is necessary to overcome
43 in order to extract information from raw EEG signals.

44 BCI has gained mainstream public awareness with worldwide challenge competitions like
45 Cybathlon (Riener and Seward, 2014; Novak et al., 2018) and even been broadcasted during the inauguration
46 ceremony of the 2014 Soccer World Cup. New developments have overcome the out-of-the-lab high-bar
47 and they are starting to be used in real world environments (Guger et al., 2017; Huggins et al., 2016).
48 However, they still lack the necessary robustness, and its performance is well behind any other method of
49 human computer interaction, including any kind of detection of residual muscular movement (Clerc et al.,
50 2016).

51 A few works have explored the idea of exploiting the signal waveform to analyze the EEG signal.
52 In (Alvarado-González et al., 2016) an approach based on Slope Horizontal Chain Code is presented,
53 whereas in (Yamaguchi et al., 2009) a similar procedure was implemented based on Mathematical
54 Morphological Analysis. The seminal work of Bandt-Pompe Permutation Entropy (Berger et al., 2017) also
55 explores succinctly this idea as a basis to establish the time series ordinal patterns. In the article (Ramele
56 et al., 2016), the authors introduce a method for classification of rhythmic EEG events like Visual Occipital
57 Alpha Waves and Motor Imagery Rolandic Central μ Rhythms using the Histogram of Gradient Orientations
58 of signal plots. Inspired in that work, we propose a novel application of the developed method to classify
59 and describe transient events, particularly the P300 Event Related Potential. The proposed approach is
60 based on the waveform analysis of the shape of the EEG signal. The signal is drawn on a bidimensional
61 image plot, vector gradients of pixels around the plot are obtained, and with them, the histogram of their
62 orientations is calculated. This histogram is a direct representation of the waveform of the signal. The
63 method is built by mimicking what regularly electroencephalographers have been performing for almost a
64 century as it is described in (Hartman, 2005): visually inspecting raw signal plots.

65 This paper reports a method to, (1) describe a procedure to capture the shape of a waveform of an ERP
66 component, the P300, using histograms of gradient orientations extracted from images of signal plots,
67 and (2) outline the way in which this procedure can be used to implement an P300-Based BCI Speller
68 application. Its validity is verified by offline processing two datasets, one of data from ALS patients and
69 another one from data of healthy subjects.

70 This article unfolds as follows: Section 2.1 is dedicated to explain the Feature Extraction method based
71 on Histogram of Gradient Orientations of the Signal Plot: Section 2.1.1 shows the preprocessing pipeline,
72 Section 2.1.2 describes the image generation of the signal plot, Section 2.1.3 presents the feature extraction

73 procedure while Section 2.1.4 introduces the Speller Matrix Letter Identification procedure. In Section 2.2,
 74 the experimental protocol is expounded. Section 3 shows the results of applying the proposed technique. In
 75 the final Section 4 we expose our remarks, conclusions and future work.

2 MATERIALS AND METHODS

76 The P300 (Farwell and Donchin, 1988; Knuth et al., 2006) is a positive deflection of the EEG signal which
 77 occurs around 300 ms after the onset of a rare and deviant stimulus that the subject is expected to attend. It
 78 is produced under the oddball paradigm (Wolpaw and E., 2012) and it is consistent across different subjects.
 79 It has a lower amplitude ($\pm 5\mu V$) compared to basal EEG activity, reaching a Signal to Noise Ratio (SNR)
 80 of around -15 db estimated based on the amplitude of the P300 response signal divided by the standard
 81 deviation of the background EEG activity (Hu et al., 2010). This signal can be used to implement a speller
 82 application by means of a Speller Matrix (Farwell and Donchin, 1988). This matrix is composed of 6 rows
 83 and 6 columns of numbers and letters. The subject can focus on one character of the matrix. Figure 1 shows
 84 an example of the Speller Matrix used in the OpenVibe open source software (Renard et al., 2010), where
 85 the flashes of rows and columns provide the deviant stimulus required to elicit this physiological response.
 86 Each time a row or a column that contains the desired letter flashes, the corresponding synchronized EEG
 87 signal should also contain the P300 signature and by detecting it, the selected letter can be identified.

88 2.1 Feature Extraction from Signal Plots

89 In this section, the signal preprocessing, the method for generating images from signal plots, the feature
 90 extraction procedure and the Speller Matrix identification are described. Figure 2 shows a scheme of the
 91 entire process.

92 2.1.1 Preprocessing Pipeline

93 The data obtained by the capturing device is digitalized and a multichannel EEG signal is constructed.

94 The 6 rows and 6 columns of the Speller Matrix are intensified providing the visual stimulus. The
 95 number of a row or column is a location. A sequence of twelve randomly permuted locations l conform an
 96 intensification sequence. The whole set of twelve intensifications is repeated k_a times.

- 97 • **Signal Enhancement:** This stage consists of the enhancement of the SNR of the P300 pattern above
 98 the level of basal EEG. The pipeline starts by applying a notch filter to the raw digital signal, a 4th
 99 degree 10 Hz lowpass Butterworth filter and finally a decimation with a Finite Impulse Response (FIR)
 100 filter of order 30 from the original sampling frequency down to 16 Hz (Krusienski et al., 2006).
- 101 • **Artifact Removal:** For every complete sequence of 12 intensifications of 6 rows and 6 columns, a
 102 basic artifact elimination procedure is implemented by removing the entire sequence when any signal
 103 deviates above/bellow $\pm 70\mu V$.
- 104 • **Segmentation:** For each of the 12 intensifications of one intensification sequence, a segment S_i^l
 105 of a window of t_{max} seconds of the multichannel signal is extracted, starting from the stimulus
 106 onset, corresponding to each row/column intensification l and to the intensification sequence i . As
 107 intensifications are permuted in a random order, the segments are rearranged corresponding to row
 108 flickering, labeled 1-6, whereas those corresponding to column flickering are labeled 7-12. Two of
 109 these segments should contain the P300 ERP signature time-locked to the flashing stimulus, one for
 110 the row, and one for the column.
- 111 • **Signal Averaging:** The P300 ERP is deeply buried under basal EEG so the standard approach to
 112 identify it is by point-to-point averaging the time-locked stacked signal segments. Hence the values

which are not related to, and not time-locked to the onset of the stimulus are canceled out (Liang and Bougrain, 2008).

This last step determines the operation of any P300 Speller. In order to obtain an improved signal in terms of its SNR, repetitions of the sequence of row/column intensification are necessary. And, at the same time, as long as more repetitions are needed, the ability to transfer information faster is diminished, so there is a trade-off that must be acutely determined.

The procedure to obtain the point-to-point averaged signal goes as follows:

1. Highlight randomly the rows and columns from the matrix. There is one row and one column that should match the letter selected by the subject.
2. Repeat step 1 k_a times, obtaining the $1 \leq l \leq 12$ segments $S_1^l(n, c), \dots, S_{k_a}^l(n, c)$, of the EEG signal where the variables $1 \leq n \leq n_{max}$ and $1 \leq c \leq C$ correspond to sample points and channel, respectively. The parameter C is the number of available EEG channels whereas $n_{max} = F_s t_{max}$ is the segment length and F_s is the sampling frequency. The parameter k_a is the number of repetitions of intensifications and it is an input parameter of the algorithm.
3. Compute the Ensemble Average by

$$x^l(n, c) = \frac{1}{k_a} \sum_{i=1}^{k_a} S_i^l(n, c) \quad (1)$$

for $1 \leq n \leq n_{max}$ and for the channels $1 \leq c \leq C$. This provide an averaged signal $x^l(n, c)$ for the twelve locations $1 \leq l \leq 12$.

2.1.2 Signal Plotting

Averaged signal segments are standardized and scaled for $1 \leq n \leq n_{max}$ and $1 \leq c \leq C$ by

$$\tilde{x}^l(n, c) = \left\lfloor \gamma \frac{(x^l(n, c) - \bar{x}^l(c))}{\hat{\sigma}^l(c)} \right\rfloor \quad (2)$$

where $\gamma > 0$ is an input parameter of the algorithm and it is related to the image scale. In addition, $x^l(n, c)$ is the point-to-point averaged multichannel EEG signal for the sample point n and for channel c . Lastly,

$$\bar{x}^l(c) = \frac{1}{n_{max}} \sum_{n=1}^{n_{max}} x^l(n, c)$$

and

$$\hat{\sigma}^l(c) = \left(\frac{1}{n_{max} - 1} \sum_{n=1}^{n_{max}} (x^l(n, c) - \bar{x}^l(c))^2 \right)^{\frac{1}{2}}$$

are the mean and estimated standard deviation of $x^l(n, c)$, $1 \leq n \leq n_{max}$, for each channel c .

Consequently, a binary image $I^{(l,c)}$ is constructed according to

$$I^{(l,c)}(z_1, z_2) = \begin{cases} 255 & \text{if } z_1 = \gamma n; z_2 = \tilde{x}^l(n, c) + z^l(c) \\ 0 & \text{otherwise} \end{cases} \quad (3)$$

with 255 being white and representing the signal's value location and 0 for black which is the background contrast, conforming a black-and-white plot of the signal. Pixel arguments $(z_1, z_2) \in \mathbb{N} \times \mathbb{N}$ iterate over the width (based on the length of the signal segment) and height (based on the peak-to-peak amplitude) of the newly created image with $1 \leq n \leq n_{max}$ and $1 \leq c \leq C$. The value $z^l(c)$ is the image vertical position where the signal's zero value has to be situated in order to fit the entire signal within the image for each channel c :

$$z^l(c) = \left\lfloor \frac{\max_n \tilde{x}^l(n, c) - \min_n \tilde{x}^l(n, c)}{2} \right\rfloor - \left\lfloor \frac{\max_n \tilde{x}^l(n, c) + \min_n \tilde{x}^l(n, c)}{2} \right\rfloor \quad (4)$$

where the minimization and maximization are carried out for n varying between $1 \leq n \leq n_{max}$, and $\lfloor \cdot \rfloor$ denote the rounding to the smaller nearest integer of the number.

In order to complete the plot $I^{(l,c)}$ from the pixels, the Bresenham (Bresenham, 1965; Ramele et al., 2016) algorithm is used to interpolate straight lines between each pair of consecutive pixels.

2.1.3 Feature Extraction: Histogram of Gradient Orientations

Hablar y explicar primero SIFT sacando info de lo que puse en la tesis. This technique is based on Lowe's SIFT method. This method is divided in two. The first part is the detector and the second is the descriptor. The descriptor is to construct an histogram of the gradient orientations obtained on each of the different patches.

We stripped away all the details which are not used and refined the procedure to enable the effective capturing of the waveform shape.

For each generated image $I^{(l,c)}$, a keypoint \mathbf{p}_k is placed on a pixel (x_{p_k}, y_{p_k}) over the image plot and a window around the keypoint is considered. A local image patch of size $X_p \times X_p$ pixels is constructed by dividing the window in 16 blocks of size $3s$ each one, where s is the scale of the local patch and it is an input parameter of the algorithm. It is arranged in a 4×4 grid and the pixel \mathbf{p}_k is the patch center, thus $X_p = 12s$ pixels.

A local representation of the signal shape within the patch can be described by obtaining the gradient orientations on each of the 16 blocks $B_{i,j}$ with $0 \leq i, j \leq 3$ and creating a histogram of gradients. This technique is based on Lowe's SIFT (Lowe, 2004) method, and it is biomimetically inspired in how the visual cortex detects shapes by analyzing orientations (Edelman et al., 1997). In order to calculate the histogram, the interval $[0, 360]$ of possible angles is divided in 8 bins, each one of 45 degrees.

Hence, for each spatial bin $0 \leq i, j \leq 3$, corresponding to the indexes of each block $B_{i,j}$, the orientations are accumulated in a 3-dimensional histogram h through the following equation:

$$h(\theta, i, j) = 3s \sum_{\mathbf{p} \in I^{(l,c)}} w_{\text{ang}}(\angle J(\mathbf{p}) - \theta) w_{ij} \left(\frac{\mathbf{p} - \mathbf{p}_k}{3s} \right) |J(\mathbf{p})| \quad (5)$$

where \mathbf{p} is a pixel from the image $I^{(l,c)}$, θ is the angle bin with $\theta \in \{0, 45, 90, 135, 180, 225, 270, 315\}$, $|J(\mathbf{p})|$ is the norm of the gradient vector in the pixel \mathbf{p} and it is computed using finite differences and $\angle J(\mathbf{p})$ is the angle of the gradient vector. The scalar $w_{\text{ang}}(\cdot)$ and vector $w_{ij}(\cdot)$ functions are linear interpolations used by Lowe (2004) and Vedaldi and Fulkerson (2010) to provide a weighting contribution to eight adjacent bins. They are calculated as

168 Explicar la trilineal interpolation mejor, y enfatizar que esta version esta publicada en el codigo, que es
 169 una variante del codigo de Vedaldi.

$$w_{ij}(\mathbf{v}) = w(v_x - x_i)w(v_y - y_j) \quad (6)$$

170 with $0 \leq i, j \leq 3$ and

$$w_{\text{ang}}(\alpha) = \sum_{r=-1}^1 w\left(\frac{8\alpha}{2\pi} + 8r\right) \quad (7)$$

171 where x_i and y_i are the spatial bin centers located in $x_i, y_j \in \{-\frac{3}{2}, -\frac{1}{2}, \frac{1}{2}, \frac{3}{2}\}$, $\mathbf{v} = (v_x, v_y)$ is a vector
 172 variable and α a scalar variable. On the other hand, r is an integer that can vary freely between $[-1, 1]$
 173 which allows the argument α to be unconstrained in terms of its values in radians. The interpolating
 174 function $w(\cdot)$ is defined as $w(z) = \max(0, |z| - 1)$.

175 These binning functions conform a trilinear interpolation that has a combined effect of sharing the
 176 contribution of each oriented gradient between their eight adjacent bins in a tridimensional cube in the
 177 histogram space, and zero everywhere else.

178 Lastly, the fixed value of 3 is a magnification factor which corresponds to the number of pixels per each
 179 block when $s = 1$. As the patch has 16 blocks and 8 bin angles are considered, for each location l and
 180 channel c a feature called *descriptor* $\mathbf{d}^{(l,c)}$ of 128 dimension is obtained.

181 Figure 3 shows an example of a patch and a scheme of the histogram computation. In (A) a plot of the
 182 signal and the patch centered around the keypoint is shown. In (B) the possible orientations on each patch
 183 are illustrated. Only the upper-left four blocks are visible. The first eight orientations of the first block, are
 184 labeled from 1 to 8 clockwise. The orientations of the second block $B_{1,2}$ are labeled from 9 to 16. This
 185 labeling continues left-to-right, up-down until the eight orientations for all the sixteen blocks are assigned.
 186 They form the corresponding descriptor \mathbf{d} of 128 coordinates. Finally, in (C) an enlarged image plot is
 187 shown where the oriented gradient vector for each pixel can be seen.

188 2.1.4 Speller Matrix letter Identification

189 2.1.4.1 P300 ERP Extraction

190 Segments corresponding to row flickering are labeled 1-6, whereas those corresponding to column
 191 flickering are labeled 7-12. The extraction process has the following steps:

- 192 • **Step A:** First highlight rows and columns from the matrix in a random permutation order and obtain
 193 the Ensemble Average as detailed in steps 1, 2 and 3 in Section 2.1.1.
- 194 • **Step B:** Plot the signals $\tilde{x}^l(n, c)$, $1 \leq n \leq n_{max}$, $1 \leq c \leq C$, according Section 2.1.2 in order to
 195 generate the images $I^{(l,c)}$ for rows and columns $1 \leq l \leq 12$.
- 196 • **Step C:** Obtain the descriptors $\mathbf{d}^{(l,c)}$ for rows and columns from $I^{(l,c)}$ in accordance to the method
 197 described in Section 2.1.3.

198 2.1.4.2 Calibration

199 A trial, as defined by the BCI2000 platform (Schalk et al., 2004), is every attempt to select just one letter
 200 from the speller. A set of trials is used for calibration and once the calibration is complete it can be used to
 201 identify new letters from new trials.

During the calibration phase, two descriptors $\mathbf{d}^{(l,c)}$ are extracted for each available channel, corresponding to the locations l of a selection of one previously instructed letter from the set of calibration trials. These descriptors are the P300 templates, grouped together in a template set called T^c . The set is constructed using the steps described in Section 2.1.1 and the steps A, B and C of the P300 ERP extraction process.

Additionally, the best performing channel, bpc is identified based on the the channel where the best Character Recognition Rate is obtained.

2.1.4.3 Letter identification

In order to identify the selected letter, the template set T^{bpc} is used as a database. Thus, new descriptors are computed and they are compared against the descriptors belonging to the calibration template set T^{bpc} .

Subir la info de que esta basado en kNN pero aclarar que esta es una variacion del algoritmo especifica y es parte de la propuesta de este paper.

- **Step D:** Match to the calibration template T^{bpc} by computing

$$row = \arg \min_{l \in \{1, \dots, 6\}} \sum_{q \in N_T(\mathbf{d}^{(l,bpc)})} \left\| q - \mathbf{d}^{(l,bpc)} \right\|^2 \quad (8)$$

and

$$col = \arg \min_{l \in \{7, \dots, 12\}} \sum_{q \in N_T(\mathbf{d}^{(l,bpc)})} \left\| q - \mathbf{d}^{(l,bpc)} \right\|^2 \quad (9)$$

where $N_T(\mathbf{d}^{(l,bpc)})$ is defined as $N_T(\mathbf{d}^{(l,bpc)}) = \{\mathbf{d} \in T^{bpc} / \text{is the } k\text{-nearest neighbor of } \mathbf{d}^{(l,bpc)}\}$ for the best performing channel. This set is obtained by sorting all the elements in T^{bpc} based on distances between them and $\mathbf{d}^{(l,bpc)}$, choosing the k with smaller values, with k a parameter of the algorithm. This procedure is based on the k-NBNN algorithm (Boiman et al., 2008).

By computing the aforementioned equations, the letter of the matrix can be determined from the intersection of the row row and column col . Figure 2 shows a scheme of this process.

2.2 Experimental Protocol

To verify the validity of the proposed framework and method, the public dataset 008-2014 (Riccio et al., 2013) published on the BNCI-Horizon website (Brunner et al., 2014) by IRCCS Fondazione Santa Lucia, is used. Additionally, an own dataset with the same experimental conditions is generated. Both of them are utilized to perform an offline BCI Simulation to decode the spelled words from the provided signals.

The algorithm is implemented using VLFeat (Vedaldi and Fulkerson, 2010) Computer Vision libraries on MATLAB V2014a (Mathworks Inc., Natick, MA, USA). Furthermore, in order to enhance the impact of our paper and for a sake of reproducibility, the code of the algorithm has been made available at: <https://bitbucket.org/itba/hist>.

In the following sections the characteristics of the datasets and parameters of the identification algorithm are described.

2.2.1 P300 ALS Public Dataset

The experimental protocol used to generate this dataset is explained in (Riccio et al., 2013) but can be summarized as follows: 8 subjects with confirmed diagnoses but on different stages of ALS disease, were recruited and accepted to perform the experiments. The Visual P300 detection task designed for this experiment consisted of spelling 7 words of 5 letters each, using the traditional P300 Speller Matrix (Farwell

and Donchin, 1988). The flashing of rows and columns provide the deviant stimulus required to elicit this physiological response. The first 3 words are used for calibration and the remaining 4 words, for testing with visual feedback. A trial is every attempt to select a letter from the speller. It is composed of signal segments corresponding to $k_a = 10$ repetitions of flashes of 6 rows and $k_a = 10$ repetitions of flashes of 6 columns of the matrix, yielding 120 repetitions. Flashing of a row or a column is performed for 0.125 s, following by a resting period (i.e. inter-stimulus interval) of the same length. After 120 repetitions an inter-trial pause is included before resuming with the following letter.

The recorded dataset was sampled at 256 Hz and it consisted of a scalp multichannel EEG signal for electrode channels Fz, Cz, Pz, Oz, P3, P4, PO7 and PO8, identified according to the 10-20 International System, for each one of the 8 subjects. The recording device was a research-oriented digital EEG device (g.Mobilab, g.Tec, Austria) and the data acquisition and stimuli delivery were handled by the BCI2000 open source software (Schalk et al., 2004).

In order to assess and verify the identification of the P300 response, subjects are instructed to perform a copy-spelling task. They have to fix their attention to successive letters for copying a previously determined set of words, in contrast to a free-running operation of the speller where each user decides on its own what letter to choose.

2.2.2 P300 for healthy subjects

We replicate the same experiment on healthy subjects using a wireless digital EEG device (g.Nautilus, g.Tec, Austria). The experimental conditions are the same as those used for the previous dataset, as detailed in section 2.2.1. The produced dataset is available in a public online repository (Ramele et al., 2017).

Participants are recruited voluntarily and the experiment is conducted anonymously in accordance with the Declaration of Helsinki published by the World Health Organization. No monetary compensation is handed out and all participants agree and sign a written informed consent. This study is approved by the *Departamento de Investigación y Doctorado, Instituto Tecnológico de Buenos Aires (ITBA)*. All healthy subjects have normal or corrected-to-normal vision and no history of neurological disorders. The experiment is performed with 8 subjects, 6 males, 2 females, 6 right-handed, 2 left-handed, average age 29.00 years, standard deviation 11.56 years, range 20-56 years.

EEG data is collected in a single recording session. Participants are seated in a comfortable chair, with their vision aligned to a computer screen located one meter in front of them. The handling and processing of the data and stimuli is conducted by the OpenVibe platform (Renard et al., 2010).

Gel-based active electrodes (g.LADYbird, g.Tec, Austria) are used on the same positions Fz, Cz, Pz, Oz, P3,P4, PO7 and PO8. Reference is set to the right ear lobe and ground is preset as the AFz position. Sampling frequency is slightly different, and is set to 250 Hz, which is the closest possible to the one used with the other dataset.

2.2.3 Parameters

The patch size is $X_P = 12s \times 12s$ pixels, where s is the scale of the local patch and it is an input parameter of the algorithm. The P300 event can have a span of 400 ms and its amplitude can reach $10\mu V$ (Rao, 2013). Hence it is necessary to utilize a signal segment of size $t_{max} = 1$ second and a size patch X_P that could capture an entire transient event. With this purpose in consideration, the s value election is essential.

We propose the Equations 10 and 11 to compute the scale value in horizontal and vertical directions, respectively.

$$s_x = \frac{\gamma \lambda F_s}{12} \quad (10)$$

$$s_y = \frac{\gamma \Delta \mu V}{12} \quad (11)$$

where λ is the length in seconds covered by the patch, F_s is the sampling frequency of the EEG signal (downsampled to 16 Hz) and $\Delta \mu V$ corresponds to the amplitude in microvolts that can be covered by the height of the patch. The geometric structure of the patch forces a squared configuration, then we discerned that by using $s = s_x = s_y = 3$ and $\gamma = 4$, the local patch and the descriptor can identify events of $9 \mu V$ of amplitude, with a span of $\lambda = 0.56$ seconds. This also determines that 1 pixel represents $\frac{1}{\gamma} = \frac{1}{4} \mu V$ on the vertical direction and $\frac{1}{F_s \gamma} = \frac{1}{64}$ seconds on the horizontal direction. The keypoints \mathbf{p}_k are located at $(x_{p_k}, y_{p_k}) = (0.55 F_s \gamma, z^l(c)) = (35, z^l(c))$ for the corresponding channel c and location l (see Equation 4). In this way the whole transient event is captured. Figure 4 shows a patch of a signal plot covering the complete amplitude (vertical direction) and the complete span of the signal event (horizontal direction).

Lastly, the number of channels C is equal to 8 for both datasets, and the number of intensification sequences k_a is fixed to 10. The parameter k used to construct the set $N_T(\mathbf{d}^{(l,c)})$ is assigned to $k = 7$, which was found empirically to achieve better results. In addition, the norm used on Equations 8 and 9 is the cosine norm, and descriptors are normalized to $[-1, 1]$.

Aclara que se hace una comparacion con SVM y SWLDA y como se construye el feature para estos casos (exactamente detallando el tamano).

3 RESULTS

Table 1 shows the results of applying the Histogram of Gradient Orientations (HIST) algorithm to the subjects of the public dataset of ALS patients. The percentage of correctly spelled letters is calculated while performing an offline BCI Simulation. From the seven words for each subject, the first three are used for calibration, and the remaining four are used for testing. The best performing channel bpc is informed as well. The target ratio is 1 : 36; hence theoretical chance level is 2.8%. It can be observed that the best performance of the letter identification method is reached in a dissimilar channel depending on the subject being studied. Table 1 and 2 show for comparison the obtained performance rates using single-channel signals with the Support Vector Machine (SVM) (Scholkopf and Smola, 2001) classifier. This method is configured to use a linear kernel. The best performing channel, where the best letter identification rate was achieved, is also depicted.

The Information Transfer Rate (ITR), or Bit Transfer Rate (BTR), in the case of reactive BCIs (Wolpaw and E., 2012) depends on the amount of signal averaging required to transmit a valid and robust selection. Figure 5 shows the performance curves for varying intensification sequences for the subjects included in the dataset of ALS patients. It can be noticed that the percentage of correctly identified letters depends on the number of intensification sequences that are used to obtain the averaged signal. Moreover, when the number of intensification sequences tend to 1, which corresponds to single-intensification character recognition, the performance is reduced. As mentioned before, the SNR of the P300 obtained from only one segment of the intensification sequence is very low and the shape of its P300 component is not very well defined.

In Table 2 the results obtained for 8 healthy subjects are shown. It can be observed that the performance is above chance level. It was verified that HIST method has an improved performance at letter identification than SVM that process the signals on a channel by channel strategy (Wilcoxon signed-rank test, $p = 0.004$ for both datasets).

Tables 3 and 4 are presented in order to compare the performance of the HIST method versus a multichannel version of the Stepwise Linear Discriminant Analysis (SWLDA) and SVM classification algorithms for both datasets. The feature was formed by concatenating all the channels (Krusienski et al., 2006). SWLDA is the methodology proposed by the ALS dataset's publisher. Since authors Riccio et al. (2013) did not report the Character Recognition Rate obtained for this dataset, we replicate their procedure and include the performance obtained with the SWLDA algorithm at letter identification. It was verified for the dataset of ALS patients that it has similar performance against other methods like SWLDA or SVM, which use a multichannel feature (Quade test with $p = 0.55$) whereas for the dataset of healthy subjects significant differences were found (Quade test with $p = 0.02$) where only the HIST method achieved a different performance than SVM (with multiple comparisons, significant difference of level 0.05).

The P300 ERP consists of two overlapping components: the P3a and P3b, the former with frontocentral distribution while the later stronger on centroparietal region (Polich, 2007). Hence, the standard practice is to find the stronger response on the central channel Cz (Riccio et al., 2013). However, Krusienski et al. (2006) show that the response may also arise in occipital regions. We found that by analyzing only the waveforms, occipital channels PO8 and PO7 show higher performances for some subjects.

As subjects have varying *latencies* and *amplitudes* of their P300 components, they also have a varying stability of the *shape* of the generated ERP (Nam et al., 2010). Figure 6 shows 10 sample P300 templates patches for patients 8 and 3 from the dataset of ALS patients. It can be discerned that in coincidence with the performance results, the P300 signature is more clear and consistent for subject 8 (A) while for subject 3 (B) the characteristic pattern is more difficult to perceive.

Additionally, the stability of the P300 component waveform has been extensively studied in patients with ALS (Sellers et al., 2006; Madarame et al., 2008; Nijboer and Broermann, 2009; Mak et al., 2012; McCane et al., 2015) where it was found that these patients have a stable P300 component, which were also sustained across different sessions. In line with these results we do not find evidence of a difference in terms of the performance obtained by analyzing the waveforms (HIST) for the group of patients with ALS and the healthy group of volunteers (Mann-Whitney U Test, $p = 0.46$). Particularly, the best performance is obtained for a subject from the ALS dataset for which, based on visual observation, the shape of they P300 component is consistently identified.

It is important to remark that when applied to binary images obtained from signal plots, the feature extraction method described in Section 2.1.3 generates sparse descriptors. Under this subspace we found that using the cosine metric yielded a significant performance improvement. On the other hand, the unary classification scheme based on the NBN algorithm proved very beneficial for the P300 Speller Matrix. This is due to the fact that this approach solves the unbalance dataset problem which is inherent to the oddball paradigm (Tibon and Levy, 2015).

4 DISCUSSION

Among other applications of Brain Computer Interfaces, the goal of the discipline is to provide communication assistance to people affected by neuro-degenerative diseases, who are the most likely population to benefit from BCI systems and EEG processing and analysis.

In this work, a method to extract an objective metric from the waveform of the plots of EEG signals is presented. Its usage to implement a valid P300-Based BCI Speller application is expounded. Additionally, its validity is evaluated using a public dataset of ALS patients and an own dataset of healthy subjects.

It was verified that this method has an improved performance at letter identification than other methods that process the signals on a channel by channel strategy, and it even has a comparable performance against other methods like SWLDA or SVM, which uses a multichannel feature. Furthermore, this method has the advantage that shapes of waveforms can be analyzed in an objective way. We observed that the shape of the P300 component is more stable in occipital channels, where the performance for identifying letters is higher. We additionally verified that ALS P300 signatures are stable in comparison to those of healthy subjects.

We believe that the use of descriptors based on histogram of gradient orientation, presented in this work, can also be utilized for deriving a shape metric in the space of the P300 signals which can complement other metrics based on time-domain as those defined by Mak et al. (2012). It is important to notice that the analysis of waveform shapes is usually performed in a qualitative approach based on visual inspection (Sellers et al., 2006), and a complementary methodology which offer a quantitative metric will be beneficial to these routinely analysis of the waveform of ERPs.

The goal of this work is to answer the question if a P300 component could be solely determined by inspecting automatically their waveforms. We conclude affirmatively, though two very important issues still remain:

First, the stability of the P300 in terms of its shape is crucial: the averaging procedure, montages, the signal to noise ratio and spatial filters all of them are non-physiological factors that affect the stability of the shape of the P300 ERP. We tested a preliminary approach to assess if the morphological shape of the P300 of the averaged signal can be stabilized by applying different alignments of the stacked segments (see Figure 2) and we verified that there is a better performance when a correct segment alignment is applied. We applied Dynamic Time Warping (DTW) (Casarotto et al., 2005) to automate the alignment procedure but we were unable to find a substantial improvement. Further work to study the stability of the shape of the P300 signature component needs to be addressed.

The second problem is the amplitude variation of the P300. We propose a solution by standardizing the signal, shown in Equation 2. It has the effect of normalizing the peak-to-peak amplitude, moderating its variation. It has also the advantage of reducing noise that was not reduced by the averaging procedure. It is important to remark that the averaged signal variance depends on the number of segments used to compute it (Van Drongelen, 2006). The standardizing process converts the signal to unit signal variance which makes it independent of the number k_a of signals averaged. Although this is initially an advantageous approach, the standardizing process reduces the amplitude of any significant P300 complex diminishing its automatic interpretation capability.

In our opinion, the best benefit of the presented method is that a closer collaboration of the field of BCI with physicians can be fostered (Chavarriaga et al., 2017), since this procedure intent to imitate human visual observation. Automatic classification of patterns in EEG that are specifically identified by their shapes like K-Complex, Vertex Waves, Positive Occipital Sharp Transient (Hartman, 2005) are a prospect future work to be considered. We are currently working in unpublished material analyzing K-Complex components that could eventually provide assistance to physicians to locate these EEG patterns, specially in long recording periods, frequent in sleep research (Michel and Murray, 2012). Additionally, it can be used for artifact removal which is performed on many occasions by visually inspecting signals. This is due to the fact that the descriptors are a direct representation of the shape of signal waveforms. In line with these applications, it can be used to build a database (Chavarriaga et al., 2017) of quantitative representations of

398 waveforms and improve atlases (Hartman, 2005), which are currently based on qualitative descriptions of
399 signal shapes.

CONFLICT OF INTEREST STATEMENT

400 The authors declare that the research was conducted in the absence of any commercial or financial
401 relationships that could be construed as a potential conflict of interest.

AUTHOR CONTRIBUTIONS

402 This work is part of the PhD thesis of RR which is directed by JS and codirected by AV.

FUNDING

403 This project was supported by the ITBACyT-15 funding program issued by ITBA University from Buenos
404 Aires, Argentina.

REFERENCES

- 405 Alvarado-González, M., Garduño, E., Bribiesca, E., Yáñez-Suárez, O., and Medina-Bañuelos, V. (2016).
406 P300 Detection Based on EEG Shape Features. *Computational and Mathematical Methods in Medicine*,
407 1–14doi:10.1155/2016/2029791
- 408 Berger, S., Schneider, G., Kochs, E., and Jordan, D. (2017). Permutation Entropy: Too Complex a Measure
409 for EEG Time Series? *Entropy* 2017, Vol. 19, Page 692 19, 692. doi:10.3390/E19120692
- 410 Boiman, O., Shechtman, E., and Irani, M. (2008). In defense of nearest-neighbor based image classification.
411 *26th IEEE Conference on Computer Vision and Pattern Recognition, CVPR* doi:10.1109/CVPR.2008.
412 4587598
- 413 Bresenham, J. E. (1965). Algorithm for computer control of a digital plotter. *IBM Systems Journal* 4,
414 25–30
- 415 Brunner, C., Blankertz, B., Cincotti, F., Kübler, A., Mattia, D., Miralles, F., et al. (2014). BNCI Horizon
416 2020 – Towards a Roadmap for Brain / Neural Computer Interaction. *Lecture Notes in Computer Science*
417 8513, 475–486
- 418 Carlson, T. and del R. Millan, J. (2013). Brain-controlled wheelchairs: A robotic architecture. *IEEE*
419 *Robotics & Automation Magazine* 20, 65–73. doi:10.1109/MRA.2012.2229936
- 420 Casarotto, S., Bianchi, A., Cerutti, S., and Chiarenza, G. (2005). Dynamic time warping in the analysis of
421 event-related potentials. *IEEE Engineering in Medicine and Biology Magazine* 24, 68–77. doi:10.1109/
422 MEMB.2005.1384103
- 423 Chavarriaga, R., Fried-Oken, M., Kleih, S., Lotte, F., and Scherer, R. (2017). Heading for new shores!
424 Overcoming pitfalls in BCI design. *Brain-Computer Interfaces* 4, 60–73. doi:10.1080/2326263X.2016.
425 1263916
- 426 Clerc, M., Bougrain, L., and Lotte, F. (2016). *Brain-computer interfaces, Technology and applications*
427 *2(Cognitive Science)* (ISTE Ltd. and Wiley)
- 428 De Vos, M. and Debener, S. (2014). Mobile EEG: Towards brain activity monitoring during natural action
429 and cognition. *International Journal of Psychophysiology* 91, 1–2. doi:10.1016/j.ijpsycho.2013.10.008
- 430 Edelman, S., Intrator, N., and Poggio, T. (1997). Complex cells and object recognition
431 Farwell, L. A. and Donchin, E. (1988). Talking off the top of your head: toward a mental prosthesis utilizing
432 event-related brain potentials. *Electroencephalography and clinical neurophysiology* 70, 510–23
- 433 Guger, C., Allison, B. Z., and Lebedev, M. A. (2017). Introduction. In *Brain Computer Interface Research:*
434 *A State of the Art Summary* 6 (Springer, Cham). 1–8. doi:10.1007/978-3-319-64373-1_1

- Guger, C., Daban, S., Sellers, E., Holzner, C., Krausz, G., Carabalona, R., et al. (2009). How many people are able to control a P300-based brain-computer interface (BCI)? *Neuroscience Letters* 462, 94–98. doi:10.1016/j.neulet.2009.06.045
- Hartman, a. L. (2005). *Atlas of EEG Patterns*, vol. 65 (Lippincott Williams & Wilkins). doi:10.1212/01.wnl.0000174180.41994.39
- Hu, L., Mouraux, A., Hu, Y., and Iannetti, G. D. (2010). A novel approach for enhancing the signal-to-noise ratio and detecting automatically event-related potentials (ERPs) in single trials. *NeuroImage* 50, 99–111. doi:10.1016/j.neuroimage.2009.12.010
- Huggins, J. E., Alcaide-Aguirre, R. E., and Hill, K. (2016). Effects of text generation on P300 brain-computer interface performance. *Brain-Computer Interfaces* 3, 112–120. doi:10.1080/2326263X.2016.1203629
- Jure, F., Carrere, L., Gentiletti, G., and Tabernig, C. (2016). BCI-FES system for neuro-rehabilitation of stroke patients. *Journal of Physics: Conference Series* 705, 1–8. doi:10.1088/1742-6596/705/1/012058
- Knuth, K. H., Shah, A. S., Truccolo, W. A., Ding, M., Bressler, S. L., and Schroeder, C. E. (2006). Differentially variable component analysis: Identifying multiple evoked components using trial-to-trial variability. *Journal of Neurophysiology* 95, 3257–3276. doi:10.1152/jn.00663.2005
- Krusienski, D. J., Sellers, E. W., Cabestaing, F., Bayoudh, S., McFarland, D. J., Vaughan, T. M., et al. (2006). A comparison of classification techniques for the P300 Speller. *Journal of Neural Engineering* 3, 299–305. doi:10.1088/1741-2560/3/4/007
- Liang, N. and Bougrain, L. (2008). Averaging techniques for single-trial analysis of oddball event-related potentials. *4th International Brain-Computer*, 1–6
- Lotte, F., Faller, J., Guger, C., Renard, Y., Pfurtscheller, G., Lécuyer, A., et al. (2013). *Combining BCI with Virtual Reality: Towards New Applications and Improved BCI* (Berlin, Heidelberg: Springer Berlin Heidelberg). 197–220. doi:10.1007/978-3-642-29746-5_10
- Lowe, G. (2004). SIFT - The Scale Invariant Feature Transform. *International Journal* 2, 91–110
- Madarame, T., Tanaka, H., Inoue, T., Kamata, M., and Shino, M. (2008). The development of a brain computer interface device for amyotrophic lateral sclerosis patients. In *Conference Proceedings - IEEE International Conference on Systems, Man and Cybernetics (IEEE)*, 2401–2406. doi:10.1109/ICSMC.2008.4811654
- Mak, J. N., McFarland, D. J., Vaughan, T. M., McCane, L. M., Tsui, P. Z., Zeitlin, D. J., et al. (2012). EEG correlates of P300-based brain-computer interface (BCI) performance in people with amyotrophic lateral sclerosis. *Journal of Neural Engineering* 9. doi:10.1088/1741-2560/9/2/026014
- McCane, L. M., Heckman, S. M., McFarland, D. J., Townsend, G., Mak, J. N., Sellers, E. W., et al. (2015). P300-based brain-computer interface (BCI) event-related potentials (ERPs): People with amyotrophic lateral sclerosis (ALS) vs. age-matched controls. *Clinical Neurophysiology* 126, 2124–2131. doi:10.1016/j.clinph.2015.01.013
- Michel, C. M. and Murray, M. M. (2012). Towards the utilization of EEG as a brain imaging tool. *NeuroImage* 61, 371–385. doi:10.1016/j.neuroimage.2011.12.039
- Nam, C. S., Li, Y., and Johnson, S. (2010). Evaluation of P300-based brain-computer interface in real-world contexts. *International Journal of Human-Computer Interaction* 26, 621–637. doi:10.1080/10447311003781326
- Nijboer, F. and Broermann, U. (2009). Brain Computer Interfaces for Communication and Control in Locked-in Patients. In *Graimann B., Pfurtscheller G., Allison B. (eds) Brain-Computer Interfaces. The Frontiers Collection*. (Springer Berlin Heidelberg). 185–201. doi:10.1007/978-3-642-02091-9_11

- Novak, D., Sigrist, R., Gerig, N. J., Wyss, D., Bauer, R., Gotz, U., et al. (2018). Benchmarking brain-computer interfaces outside the laboratory: The cybathlon 2016. *Frontiers in Neuroscience* 11, 756. doi:10.3389/fnins.2017.00756
- Polich, J. (2007). Updating P300: An integrative theory of P3a and P3b. *Clinical Neurophysiology* 118, 2128–2148. doi:10.1016/j.clinph.2007.04.019
- Ramele, R., Villar, A. J., and Santos, J. M. (2016). BCI classification based on signal plots and SIFT descriptors. In *4th International Winter Conference on Brain-Computer Interface, BCI 2016* (Yongpyong: IEEE), 1–4. doi:10.1109/IWW-BCI.2016.7457454
- [Dataset] Ramele, R., Villar, A. J., and Santos, J. M. (2017). P300-dataset rrid scr_015977. <https://www.kaggle.com/rramele/p300samplingdataset>
- Rao, R. P. N. (2013). *Brain-Computer Interfacing: An Introduction* (New York, NY, USA: Cambridge University Press)
- Renard, Y., Lotte, F., Gibert, G., Congedo, M., Maby, E., Delannoy, V., et al. (2010). OpenViBE: An Open-Source Software Platform to Design, Test, and Use Brain-Computer Interfaces in Real and Virtual Environments. *Presence: Teleoperators and Virtual Environments* 19, 35–53. doi:10.1162/pres.19.1.35
- Riccio, A., Simione, L., Schettini, F., Pizzimenti, A., Inghilleri, M., Belardinelli, M. O., et al. (2013). Attention and P300-based BCI performance in people with amyotrophic lateral sclerosis. *Frontiers in Human Neuroscience* 7, 732. doi:10.3389/fnhum.2013.00732
- Riener, R. and Seward, L. J. (2014). Cybathlon 2016. *2014 IEEE International Conference on Systems, Man, and Cybernetics (SMC)*, 2792–2794. doi:10.1109/SMC.2014.6974351
- Schalk, G., McFarland, D. J., Hinterberger, T., Birbaumer, N., and Wolpaw, J. R. (2004). BCI2000: a general-purpose brain-computer interface (BCI) system. *IEEE transactions on bio-medical engineering* 51, 1034–43. doi:10.1109/TBME.2004.827072
- Scholkopf, B. and Smola, A. J. (2001). *Learning with kernels: support vector machines, regularization, optimization, and beyond* (MIT press)
- Schomer, D. L. and Silva, F. L. D. (2010). *Niedermeyer's Electroencephalography: Basic Principles, Clinical Applications, and Related Fields* (Walters Kluwer -Lippincott Williams & Wilkins)
- Sellers, E. W., Kübler, A., and Donchin, E. (2006). Brain-computer interface research at the University of South Florida cognitive psychophysiology laboratory: The P300 speller. *IEEE Transactions on Neural Systems and Rehabilitation Engineering* 14, 221–224. doi:10.1109/TNSRE.2006.875580
- Tibon, R. and Levy, D. A. (2015). Striking a balance: analyzing unbalanced event-related potential data. *Frontiers in psychology* 6, 555. doi:10.3389/fpsyg.2015.00555
- Van Drongelen, W. (2006). *Signal processing for neuroscientists: an introduction to the analysis of physiological signals* (Academic press)
- Vedaldi, A. and Fulkerson, B. (2010). VLFeat - An open and portable library of computer vision algorithms. *Design* 3, 1–4. doi:10.1145/1873951.1874249
- Wolpaw, J. and E., W. (2012). *Brain-Computer Interfaces: Principles and Practice* (Oxford University Press)
- Yamaguchi, T., Fujio, M., Inoue, K., and Pfurtscheller, G. (2009). Design method of morphological structural function for pattern recognition of EEG signals during motor imagery and cognition. In *Fourth International Conference on Innovative Computing, Information and Control (ICICIC)*. 1558–1561. doi:10.1109/ICICIC.2009.161

Table 1. Character recognition rates for the public dataset of ALS patients using the Histogram of Gradient (HIST) calculated from single-channel plots. Performance rates using single-channel signals with the SVM classifier are shown for comparison. The best performing channel *bpc* for each method is visualized

Participant	<i>bpc</i>	HIST	<i>bpc</i>	Single Channel SVM
1	Cz	35%	Cz	15%
2	Fz	85%	PO8	25%
3	Cz	25%	Fz	5%
4	PO8	55%	Oz	5%
5	PO7	40%	P3	25%
6	PO7	60%	PO8	20%
7	PO8	80%	Fz	30%
8	PO7	95%	PO7	85%

Table 2. Character recognition rates for the own dataset of healthy subjects using the Histogram of Gradient (HIST) calculated from single-channel plots. Performance rates using single-channel signals with the SVM classifier are shown for comparison. The best performing channel *bpc* for each method is visualized.

Participant	<i>bpc</i>	HIST	<i>bpc</i>	Single Channel SVM
1	Oz	40%	Cz	10%
2	PO7	30%	Cz	5%
3	P4	40%	P3	10%
4	P4	45%	P4	35%
5	P4	60%	P3	10%
6	Pz	50%	P4	25%
7	PO7	70%	P3	30%
8	P4	50%	PO7	10%

Table 3. Character recognition rates and the best performing channel *bpc* for the public dataset of ALS patients using the Histogram of Gradient (HIST) (repeated here for comparison purposes). Performance rates obtained by SWLDA and SVM classification algorithms with a multichannel concatenated feature.

Participant	<i>bpc</i> for HIST	HIST	Multichannel SWLDA	Multichannel SVM
1	Cz	35%	45%	40%
2	Fz	85%	30%	50%
3	Cz	25%	65%	55%
4	PO8	55%	40%	50%
5	PO7	40%	35%	45%
6	PO7	60%	35%	70%
7	PO8	80%	60%	35%
8	PO7	95%	90%	95%

Table 4. Character recognition rates and the best performing channel *bpc* for the own dataset of healthy subjects using the Histogram of Gradient (HIST) (repeated here for comparison purposes). Performance rates obtained by SWLDA and SVM classification algorithms with a multichannel concatenated feature.

Participant	<i>bpc</i> for HIST	HIST	Multichannel SWLDA	Multichannel SVM
1	Oz	40%	65%	40%
2	PO7	30%	15%	10%
3	P4	40%	50%	25%
4	P4	45%	40%	20%
5	P4	60%	30%	20%
6	Pz	50%	35%	30%
7	PO7	70%	25%	30%
8	P4	50%	35%	20%

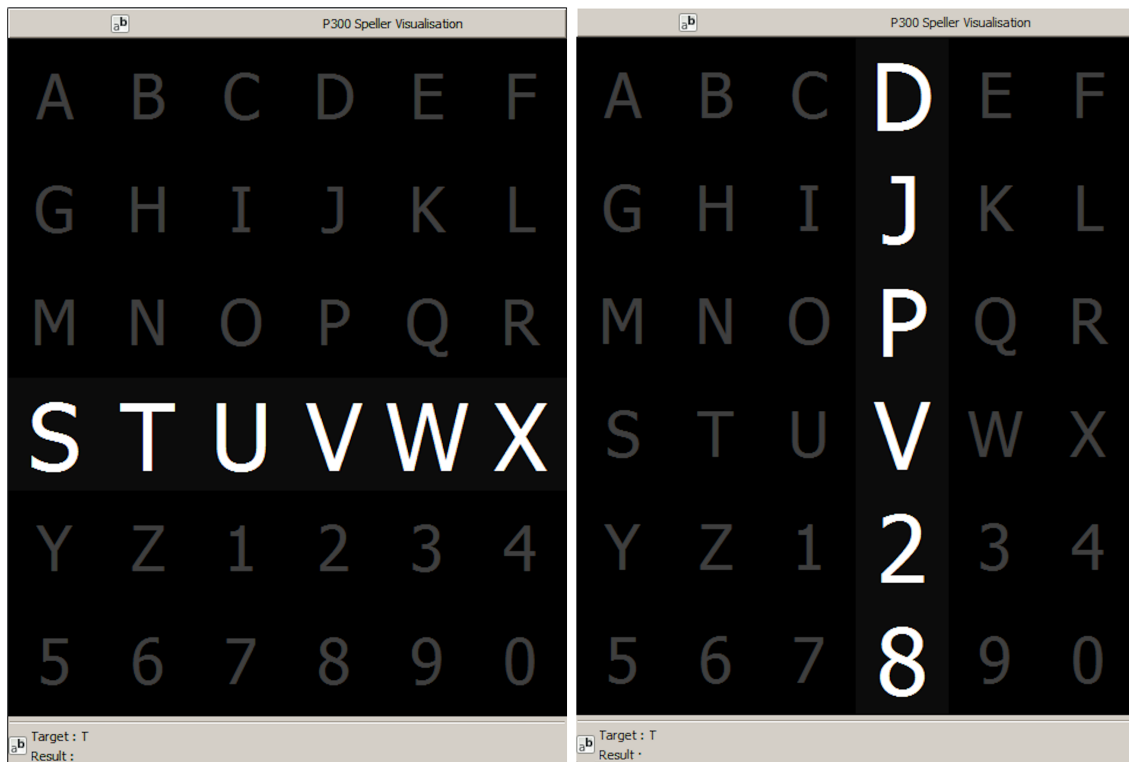


Figure 1. Example of the 6×6 Speller Matrix used in the study obtained from the OpenVibe software. Rows and columns flash in random permutations.

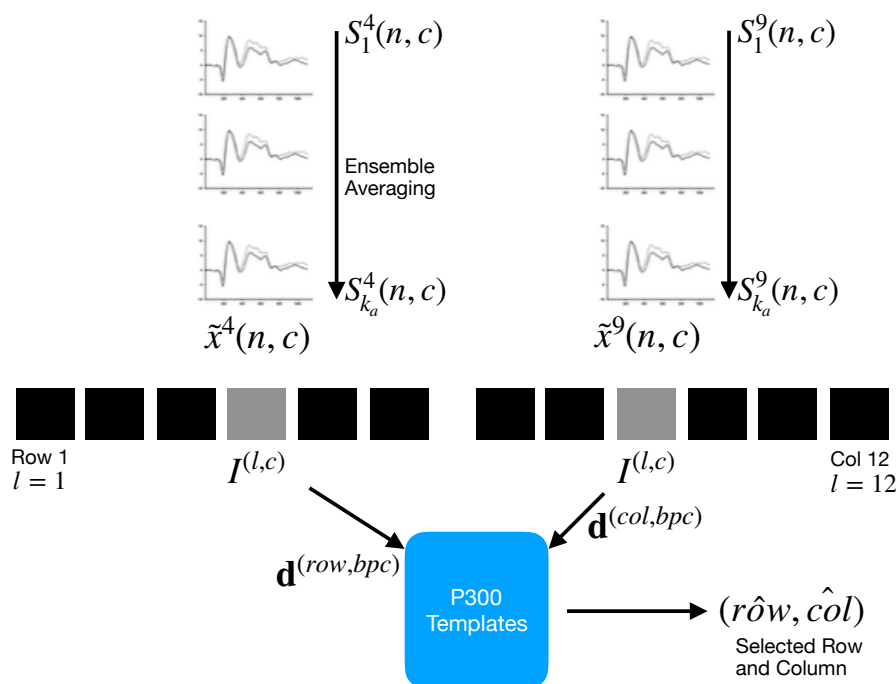


Figure 2. For each column and row, an averaged, standardized and scaled signal $\tilde{x}^l(n, c)$ is obtained from the segments S_i^l corresponding to the k_a intensification sequences with $1 \leq i \leq k_a$ and location l varying between 1 and 12. From the averaged signal, the image $I^{(l, c)}$ of the signal plot is generated and each descriptor is computed. By comparing each descriptor against the set of templates, the P300 ERP can be detected, and finally the desired letter from the matrix can be inferred.

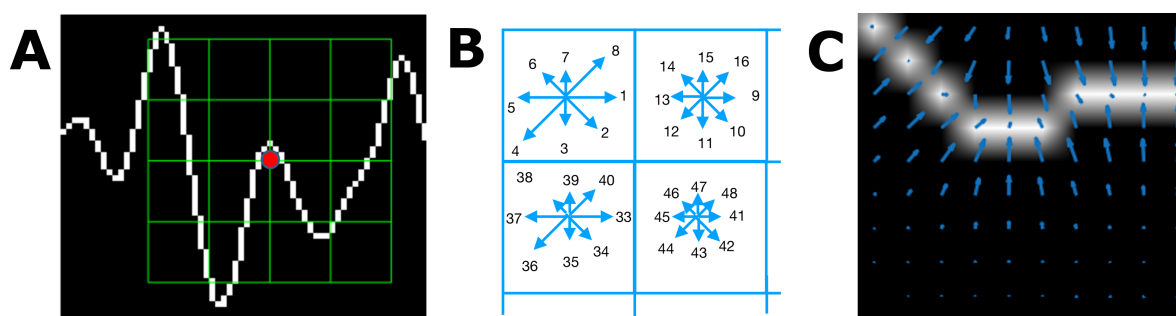


Figure 3. (A) Example of a plot of the signal, a keypoint and the corresponding patch. (B) A scheme of the orientation's histogram computation. Only the upper-left four blocks are visible. The first eight orientations of the first block, are labeled from 1 to 8 clockwise. The orientation of the second block $B_{1,2}$ is labeled from 9 to 16. This labeling continues left-to-right, up-down until the eight orientations for all the sixteen blocks are assigned. They form the corresponding descriptor of 128 coordinates. The length of each arrow represent the value of the histogram on each direction for each block. (C) Vector field of oriented gradients. Each pixel is assigned an orientation and magnitude calculated using finite differences.

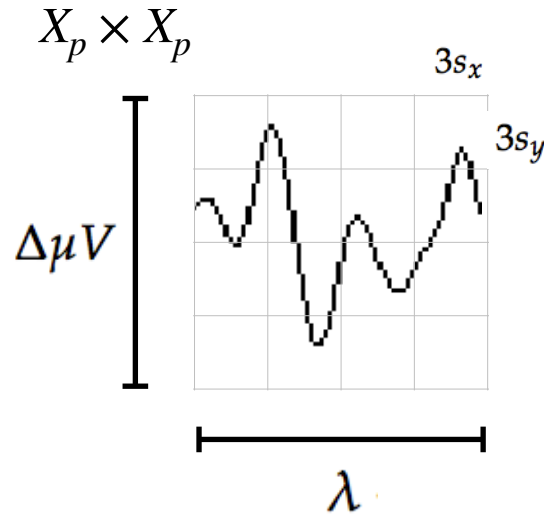


Figure 4. The scale of local patch is selected in order to capture the whole transient event. The size of the patch is $X_p \times X_p$ pixels. The vertical size consists of 4 blocks of size $3s_y$ pixels which is high enough as to contain the signal $\Delta\mu V$, the peak-to-peak amplitude of the transient event. The horizontal size includes 4 blocks of $3s_x$ and covers the entire duration in seconds of the transient signal event, λ .

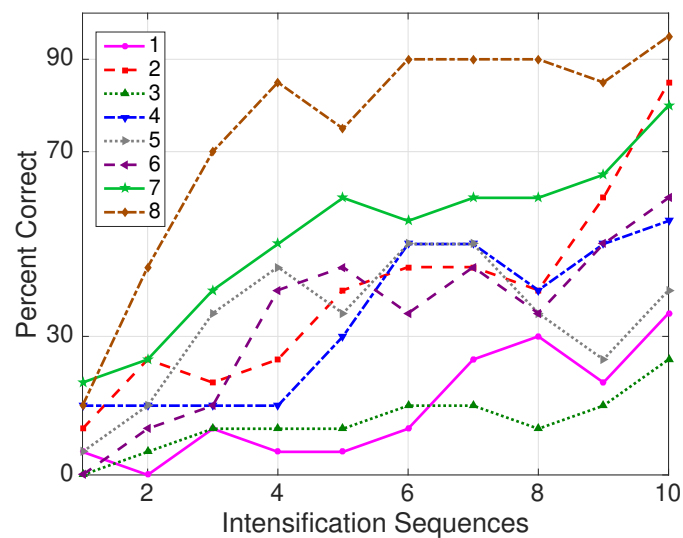


Figure 5. Performance curves for the eight subjects included in the dataset of ALS patients. Three out of eight subjects achieved the necessary performance to implement a valid P300 speller.

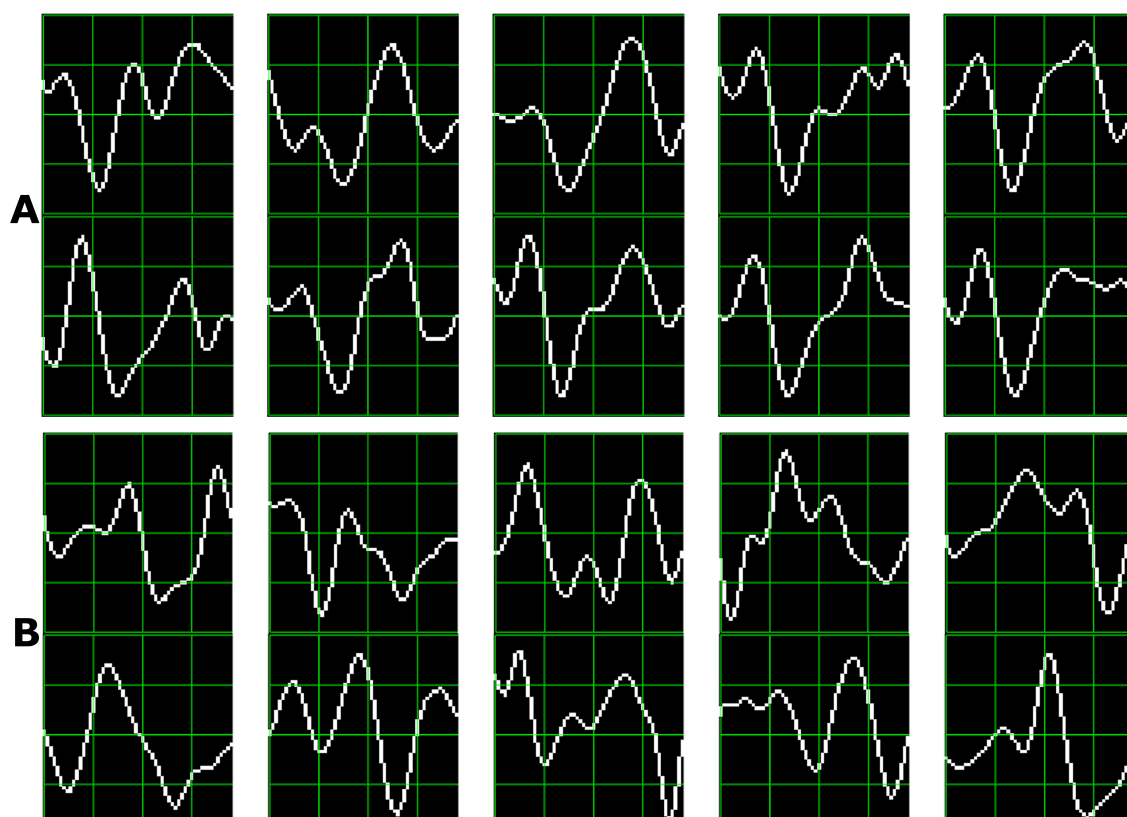


Figure 6. Ten sample P300 template patches for subjects 8 (A) and 3 (B) of the ALS Dataset. Downward deflection is positive polarity.